Contribution of unparticles to the Møller scattering in the Randall-Sundrum model

Dang Van Soa[1,†], **Le Mai Dung**[2] **and Dao Thi Le Thuy**[2]

[1]*Faculty of Applied Ssciences, University of Economics - Technology for Industries,*
456 Nguyen Thi Minh Khai, Vinh Tuy, Hai Ba Trung, Hanoi, Vietnam

[2]*Hanoi National University of Education,*
136 Xuan Thuy, Cau Giay, Hanoi, Vietnam

E-mail: [†]soadangvan@gmail.com

Abstract. *The influence of vector, scalar unparticle exchange and photon (γ), Z boson, Higgs-radion (h, ϕ) exchange on the fundamental Møller scattering in Randall-Sundrum model is presented. We evaluated the contribution from each exchange in standard model physics and unparticle physics to the final production cross-sections with the apposite energy reach in the current accelerators and colliders. The results indicate that the effect of vector unparticles is larger than its scalar all over the range of collision energy, as much greater than Higgs (h) and radion (ϕ) in the low energy. Z boson exchange also contributes the greatest to the process in both unpolarized and polarized conditions in higher energy regions when compared to photon exchange (γ) which normally dominates at the lower energies.*

Keywords: Møller scattering; scalar unparticle; vector unparticle; Randall-Sundrum model; cross-section.

Classification numbers: 12.20.-m; 14.80.Bn.

1. Introduction

Møller scattering is one of the most fundamental processes in quantum electrodynamics and various important modern experiments requiring high precision due to its entirely pointlike character. When it comes to testing the Standard Model (SM), it is also the dominant physical process in low energy electron scattering experiments [1, 2]. Thus, it plays a crucial role in the design of electron scattering experiments that search for new physics beyond the SM [3]. Additionally, the radiative Møller scattering can produce very large and complex backgrounds in the collider. Besides, the electron-electron scattering is a basic part of precision luminosity monitoring in electron scattering experiments [4, 5].

The Randall-Sundrum model (RS model) [6] was devised by L. Randall and R. Sundrum to address the Higgs Hierarchy Problem in particle physics. It has arisen extensive interest from both theoreticians and phenomenologists ever since and remained a useful tool to explore the physics of extra dimensions and sectors beyond the SM. The Hierarchy Problem emerged in quantum field theory due to the fact that the quadratic corrections divergent are applied to the Higgs field mass. These corrections require a fine-tuning so as to get the expected mass of a few hundreds GeV. The model simply changes the Hierarchy Problem into the discrepancy problem between the large size of the extra dimensions $R \simeq 1$ mm and the natural value $R \simeq l_{Pl} \simeq 10^{-3}$ cm [6]. The model assumes that on each of the boundaries of S^1/Z_2 orbifold stand two worlds with $3+1$ dimensions. Analogous to the membranes enclosing a volume, these two worlds enclosing the bulk are called 3-branes which are IR and UV brane. The SM field is localized at the former brane and the gravity is at the latter one. The distance r between the two branes creates a new scalar quantum field called the radion (φ). We have the following background metric in RS model parameterized by $ds^2 = e^{-2k|y|}\eta_{\mu\nu}dx^\mu dx^\nu + dy^2$ where $\eta_{\mu\nu} = diag(-1,1,1,1)$ is the 4D Minkowski metric, the warp factor is $e^{-2k|y|}$, written as an exponential for convenience, and k is the curvature parameter with the Planck scale order. Unlike the Kaluza-Klein metrics, the warp factor depends on the coordinate y of the extra dimension, which causes it to be non-factorizable. Moreover, this metric cannot be expressed as a product of the Minkowski metric four dimension and an extra dimension manifold. An action operator introduces the mixing of the radion and Higgs field, as the Higgs is localized on the TeV brane

$$S_\xi = \xi \int d^4x \sqrt{g_{vis}} R(g_{vis}) \hat{H}^\dagger \hat{H}, \tag{1}$$

where $R(g_{vis})$ is the Ricci scalar for the induced metric on the IR brane and H is the Higgs field in the 5D before rescaling to canonical normalization. The mass eigenstates, h and φ, are achieved through diagonalization and canonical normalization of the kinetic and mass terms in the Higgs-radion Lagrangian. The mathematical procedures and results for diagonalization could be found in [7, 8]. One finds the following

$$\begin{aligned} h_0 &= dh + c\varphi, \\ -\varphi_0 &= a\varphi + bh, \end{aligned} \tag{2}$$

where

$$\begin{aligned} a &= \frac{-\cos\theta}{Z}, \quad b = \frac{\sin\theta}{Z}, \\ c &= \sin\varphi - t\cos\varphi, \quad d = \cos\theta - t\sin\varphi, \end{aligned} \tag{3}$$

with $t = 6\xi\gamma/Z$, $Z^2 = 1 + 6\xi\gamma^2(1-6\xi)$ and $\tan 2\theta = 12\gamma\xi Z m_{h_0}^2/(m_{\varphi_0}^2 - m_{h_0}^2[Z^2 - 36\xi^2\gamma^2])$. The Higgs and radion masses before mixing are m_{φ_0}, m_{h_0}. The diagonalization stability imposes restrictions on the possible values of the mixing parameter ξ as a function of the final eigenstate masses of Higgs and radion. The ratio $\gamma \equiv v_0/\Lambda_\varphi (v_0 = 246\ GeV)$ with v_0 being the SM Higgs vacuum expectation value (VEV), which decides the restrictions.

The unparticles come from the high energy sector beyond the SM, it is probable that they transform as a singlet in the gauge group of the SM. According to H. Georgi [7], unparticles with scale dimension look like a non-integral number of invisible particles. Its dependence on the nature of the operator O_{BZ} motivated by the Banks-Zaks theory and the dimensional transmutation results in unparticles with different Lorentz formations. Below a specific scale Λ_U, the operator matches to unparticle operator with scale dimension d_U. At low energy, the interaction operator between SM particles (via operator O_{SM} with the dimension d_{SM}) and unparticles has the following form $\lambda\Lambda_U^{4-d_{SM}-d_U}O_{SM}O_U$. Phenomenologically, one works with the effective coupling which has been studied by many authors. The derivation of the virtual unparticle propagator is based on its nature of scale variance. We have the propagator for unparticle as follows

$$\Delta_F(P^2) = \frac{A_{d_U}}{2\sin(d_U\pi)}(-P^2)^{d_U-2},\tag{4}$$

where the complex function is analytic for negative P^2 :(i) if P^2 is real and negative and (ii) if P^2 is positive with an infinitesimal $i0^+$.

$$(-P^2)^{d_U-2} = \begin{cases} |P^2|^{d_U-2} \\ |P^2|^{d_U-2}e^{-id_U\pi} \end{cases}.\tag{5}$$

The vector propagators can be derived from unparticle propagator by using spectral decomposition

$$[\Delta_F(P^2)]_{\mu\nu} = \frac{A_{d_U}}{2\sin(d_U\pi)}(-P^2)^{d_U-2}\pi_{\mu\nu}(P).\tag{6}$$

The effective interactions that content the gauge symmetry group in the SM for the scalar and vector unparticle operators with standard model fields are given by

$$\begin{aligned} &\lambda_0\frac{1}{\Lambda_U^{d_U-1}}\bar{f}fO_U, \ \lambda_0\frac{1}{\Lambda_U^{d_U-1}}i\bar{f}\gamma^5 fO_U, \ \lambda_0\frac{1}{\Lambda_U^{d_U}}\bar{f}\gamma^\mu f(\partial_\mu O_U), \ \lambda_0\frac{1}{\Lambda_U^{d_U}}G_{\alpha\beta}G^{\alpha\beta}O_U \\ &\lambda_1\frac{1}{\Lambda_U^{d_U-1}}\bar{f}\gamma^\mu fO_U^\mu, \ \lambda_1\frac{1}{\Lambda_U^{d_U-1}}\bar{f}\gamma_\mu\gamma_5 fO_U^\mu, \end{aligned}\tag{7}$$

where d_U is the scaling dimension of the unparticle operators O_U, λ_0, λ_1 are the dimensionless effective coupling constants for scalar and vector unparticle operators. $G_{\alpha\beta}$ denotes the gauge field strength and f is a standard model fermion.

2. Møller scattering

With the effective couplings and the unparticle propagators, we have four t- and u-channel Feynman diagrams in Fig. 1. Apart from two standard model exchanges (γ, Z), four tree-level diagrams contain scalar and vector unparticle exchanges with Higgs-radion exchange in RS model.
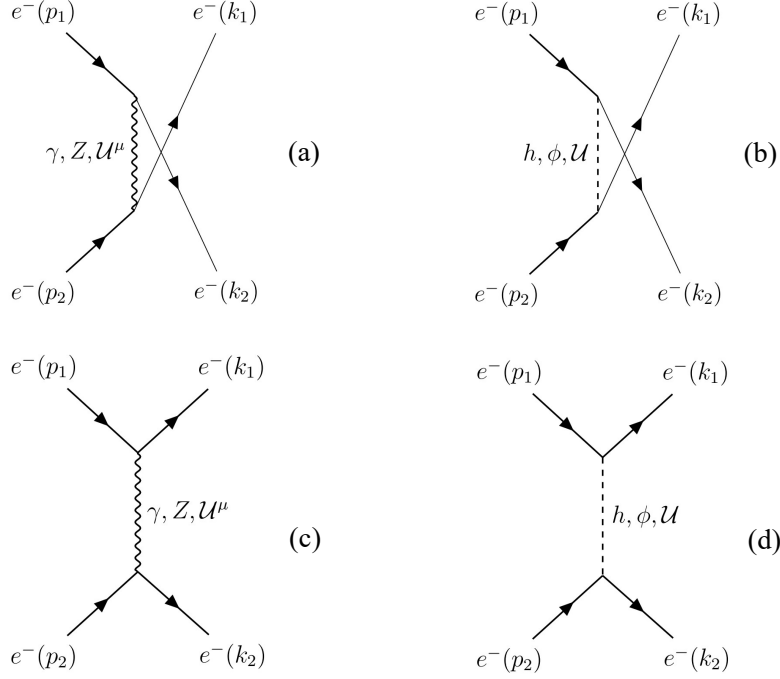
Fig. 1. Tree-level Feynman diagrams for Møller scattering in the presence of the unparticle interaction couplings in RS model.

The unpolarization scattering amplitudes for u-channel in Fig. 1 are given by

$$M_{u\gamma} = \frac{ie^2}{q_u^2} \bar{u}(k_2)\gamma_\mu u(p_1)\bar{u}(k_1)\gamma^\mu u(p_2), \tag{8}$$

$$M_{uZ} = \left(\frac{g}{4\cos\theta_W}\right)^2 \frac{i}{q_u^2 - m_Z^2}\left[g_{\mu\nu} - \frac{q_{u\mu}q_{u\nu}}{m_Z^2}\right]$$
$$\times \bar{u}(k_2)(\gamma^\nu)[(-1+4s_W^2)+\gamma_5]u(p_1)\bar{u}(k_1)(\gamma^\mu)[(-1+4s_W^2)+\gamma_5]u(p_2), \tag{9}$$

$$M_{u\mathcal{U}^\mu} = -\left(\frac{\lambda_1}{\Lambda_U^{d_U-1}}\right)^2 \frac{A_{d_U}\left(-q_u^2\right)^{d_U-2}}{2\sin(d_U\pi)}\left[-g_{\mu\nu} + \frac{q_{u\mu}q_{u\nu}}{q_u^2}\right]$$
$$\times \bar{u}(k_2)(\gamma^\nu + \gamma^\nu\gamma_5)u(p_1)\bar{u}(k_1)(\gamma^\mu + \gamma^\mu\gamma_5)u(p_2), \tag{10}$$

$$M_{uh} = -i\left(\frac{g}{2}\left[\frac{m_e}{m_W}(d+\gamma b)\right]\right)^2 \frac{1}{q_u^2 - m_h^2}\bar{u}(k_2)u(p_1)\bar{u}(k_1)u(p_2), \tag{11}$$

$$M_{u\varphi} = -i\left(\frac{g}{2}\left[\frac{m_e}{m_W}(c+\gamma a)\right]\right)^2 \frac{1}{q_u^2 - m_\varphi^2}\bar{u}(k_2)u(p_1)\bar{u}(k_1)u(p_2), \tag{12}$$

$$M_{u\mathcal{U}} = -\frac{A_{d_U}\left(-q_u^2\right)^{d_U-2}}{2\sin(d_U\pi)}\left(\frac{\lambda_0}{\Lambda_U^{d_U-1}}\right)^2 \bar{u}(k_2)\left(1+i\gamma_5 - \frac{i\hat{q}_u}{\Lambda_U}\right)u(p_1)\bar{u}(k_1)\left(1+i\gamma_5 - \frac{i\hat{q}_u}{\Lambda_U}\right)u(p_2). \tag{13}$$

The unpolarization scattering amplitudes for t-channel in Fig. 1 are given by

$$M_{t\gamma} = \frac{ie^2}{q_t^2} \bar{u}(k_1)\gamma_\mu u(p_1)\bar{u}(k_2)\gamma^\mu u(p_2),$$ (14)

$$M_{tZ} = \left(\frac{g}{4\cos\theta_W}\right)^2 \frac{i}{q_t^2 - m_Z^2}\left[g_{\mu\nu} - \frac{q_{t\mu}q_{t\nu}}{m_Z^2}\right]$$
$$\times \bar{u}(k_1)(\gamma^\nu)[(-1+4s_W^2)+\gamma_5]u(p_1)\bar{u}(k_2)(\gamma^\mu)[(-1+4s_W^2)+\gamma_5]u(p_2),$$ (15)

$$M_{tU^\mu} = -\left(\frac{\lambda_1}{\Lambda_U^{d_U-1}}\right)^2 \frac{A_{d_U}\left(-q_t^2\right)^{d_U-2}}{2\sin(d_U\pi)}\left[-g_{\mu\nu}+\frac{q_{t\mu}q_{t\nu}}{q_t^2}\right]$$
$$\times \bar{u}(k_1)(\gamma^\nu+\gamma^\nu\gamma_5)u(p_1)\bar{u}(k_2)(\gamma^\mu+\gamma^\mu\gamma_5)u(p_2),$$ (16)

$$M_{th} = -i\left(\frac{g}{2}\left[\frac{m_e}{m_W}(d+\gamma b)\right]\right)^2 \frac{1}{q_t^2-m_h^2}\bar{u}(k_1)u(p_1)\bar{u}(k_2)u(p_2),$$ (17)

$$M_{t\varphi} = -i\left(\frac{g}{2}\left[\frac{m_e}{m_W}(c+\gamma a)\right]\right)^2 \frac{1}{q_t^2-m_\varphi^2}\bar{u}(k_1)u(p_1)\bar{u}(k_2)u(p_2),$$ (18)

$$a,b,c,d$$

$$M_{tU} = -\frac{A_{d_U}\left(-q_t^2\right)^{d_U-2}}{2\sin(d_U\pi)}\left(\frac{\lambda_0}{\Lambda_U^{d_U-1}}\right)^2 \bar{u}(k_1)\left(1+i\gamma_5-\frac{i\hat{q}_t}{\Lambda_U}\right)u(p_1)\bar{u}(k_2)\left(1+i\gamma_5-\frac{i\hat{q}_t}{\Lambda_U}\right)u(p_2),$$ (19)

where $q_u = k_1 --p_2 = p_1 --k_2$, $q_t = k_2 --p_2 = p_1 --k_1$, a, b, c, d are real coefficients from Higgs-radion mixing and $\gamma \equiv v_0/\Lambda_\varphi$. The mathematical calculation is performed in the center of mass (CM) frame of the incoming beams, denoted by the 4-momenta p_1^μ and p_2^μ and the outgoing electron beams with the 4-momenta k_2 and k_1, respectively. In this frame, we have

$$p_1^\mu(E_1,\vec{p}_1),\ p_2^\mu(E_2,\vec{p}_2),\ k_1\left(E_3,\vec{k}_1\right),\ k_2\left(E_4,\vec{k}_2\right),$$
$$\vec{p}_1+\vec{p}_2 = \vec{k}_1+\vec{k}_2 = 0,\ \vec{p}_1 = \vec{p},\ \vec{p}_2 = -\vec{p},\ \vec{k}_1 = \vec{k},\ \vec{k}_2 = -\vec{k},$$ (20)
$$E_1+E_2 = E_3+E_4 = \sqrt{s}$$

where $\sqrt{s}$ is the center-of-mass energy, $\vec{k}$ and $\vec{p}$ are momentum vectors in the initial and final state in the CM frame. After primary calculations of each squared matrix elements, the differential cross-section equation [9] is given by

$$\frac{d\sigma}{d\cos\theta} = \frac{1}{32\pi s}\frac{|\vec{k}|}{|\vec{p}|}|\overline{M}|^2.$$ (21)

3. The cross-section of the Møller scattering

For numerical evaluations, we use the following parameters: the vacuum expectation of the radion field $\Lambda_\varphi = 5$ TeV [7], the radion mass is $m_\varphi = 10$ GeV [10], the Higgs mass $m_h = 125$ GeV and the mixing parameter $\xi = 1/6$. The unparticles parameters are: $\Lambda_U = 1000$ GeV, $\lambda_0 = \lambda_1 = 1$

and the scaling dimenstion $d_U = 1.7$ [11]. From the aspects of RS model and scalar unparticle physics, evaluations in dependence on more parameters are studied in [12, 13].
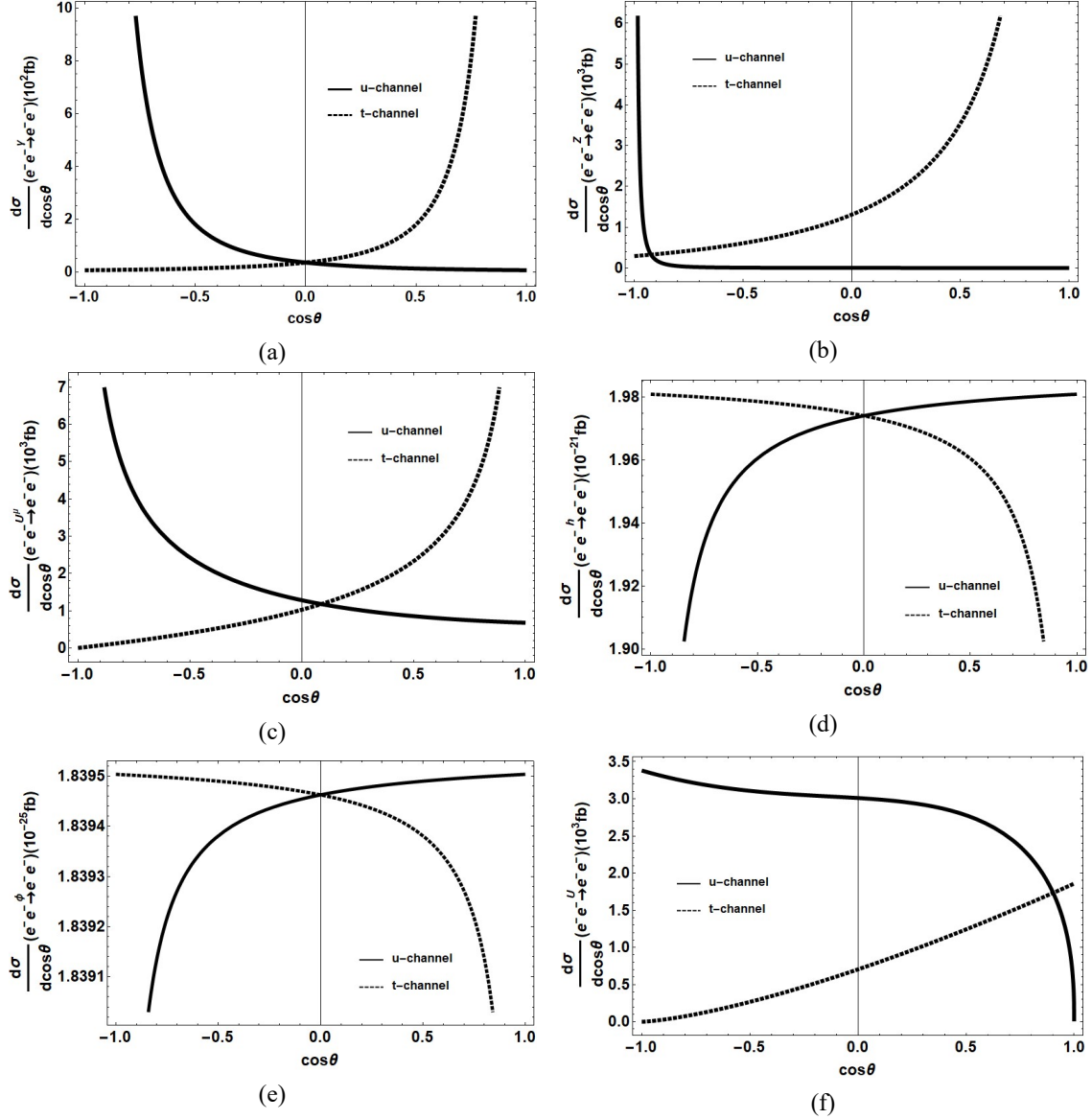
Fig. 2. Differential cross-sections as functions of $\cos\theta$ in u- and t- channel via $\gamma, Z, U^\mu, h, \varphi, U$ exchange, from 2a to 2f, respectively.

From the plots of the differential cross-sections (DCS) versus the cosine function of scattering angles (Fig. 2a-2c), the DCS via (γ, Z, U^μ) exchange (Fig. 1a, 1c) rise to the highest in two opposite directions through u- and t-channel. In u- and t-channel, the vector unparticles contribute

greater than the other exchanges at $7 \times 10^3 fb$ (Fig. 2c), while Z exchange contribution stands behind, over $6 \times 10^3 fb$ (Fig. 2b).

As for the next plots in Figs. 2d, 2e, 2f which correspond to (h, φ, U) exchange (Fig. 1b, 1d), the same DCS pattern versus the cosine functions as the DCS of (γ, Z, U^μ) exchange contribution can be seen. The highest values of DCS figures in two channels are observed in opposite directions in channel t and u via scalar unparticle exchange around $1.9 \times 10^3 fb$ and $3.4 \times 10^3 fb$, respectively. Higgs-radion effect is trivial due to weak interactions with the SM sector, the scalar unparticle exchange contribute greater than (h, φ) exchange (Fig. 2f).

(a)

(b)

(c)
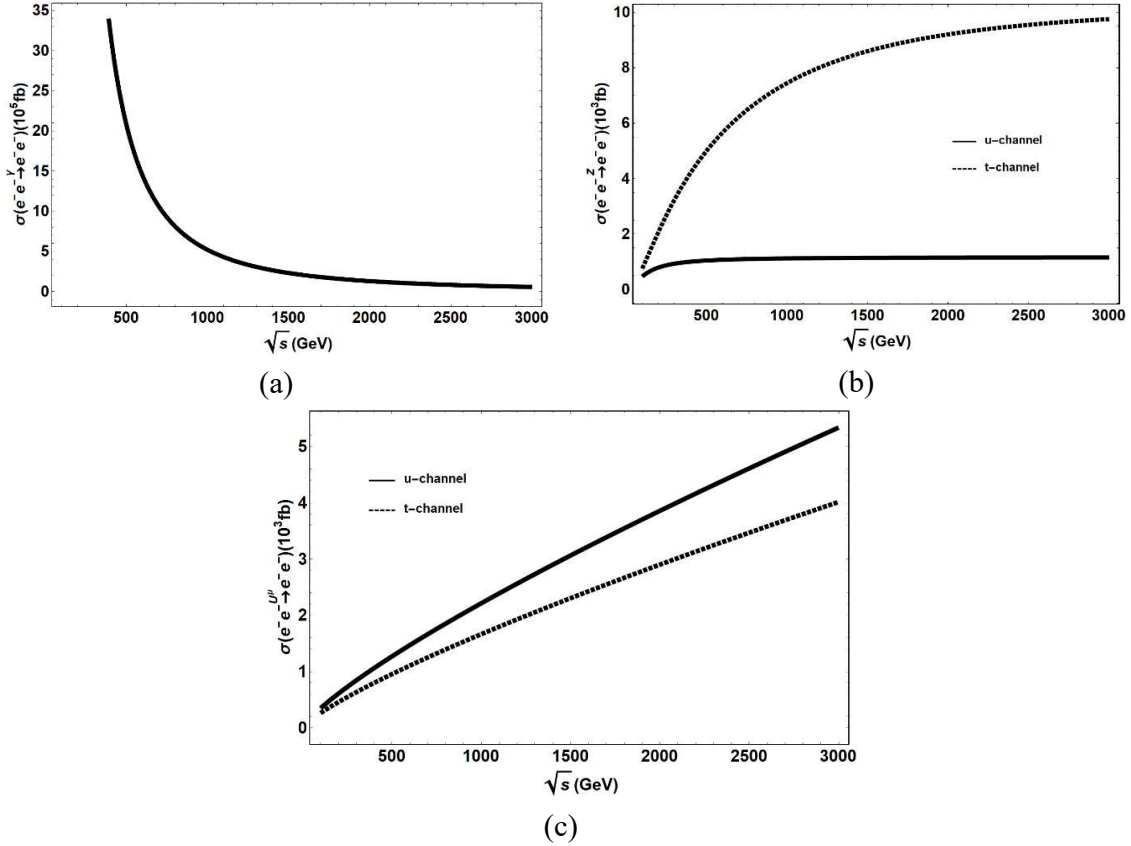
Fig. 3. Total cross-sections as functions of the collision energy via (γ, Z, U^μ) exchange.

In Fig. 3, we investigate the dependence of the total cross-sections (TCS) on the collision energy $\sqrt{s}$ in a broad range of energy scale from 0.1 to 3 TeV. From the standard model perspective, one can see two different behaviours of the TCS in high energy reach (Fig. 3a and 3b). Overall, the figures via γ exchange dominate low energy below 2 TeV, decreasing significantly in the very high energy, whereas Z exchange contribution increases albeit rather steadily in u-channel (Fig. 3b). In addition, Z exchange through t-channel also makes large contribution, around $8 - 9 \times 10^3 fb$ at very high energy above 1.5 TeV. The effect from vector unparticle exchange becomes more effective in higher energy region with a sharper rise in line with the energy $\sqrt{s}$ (Fig. 3c).
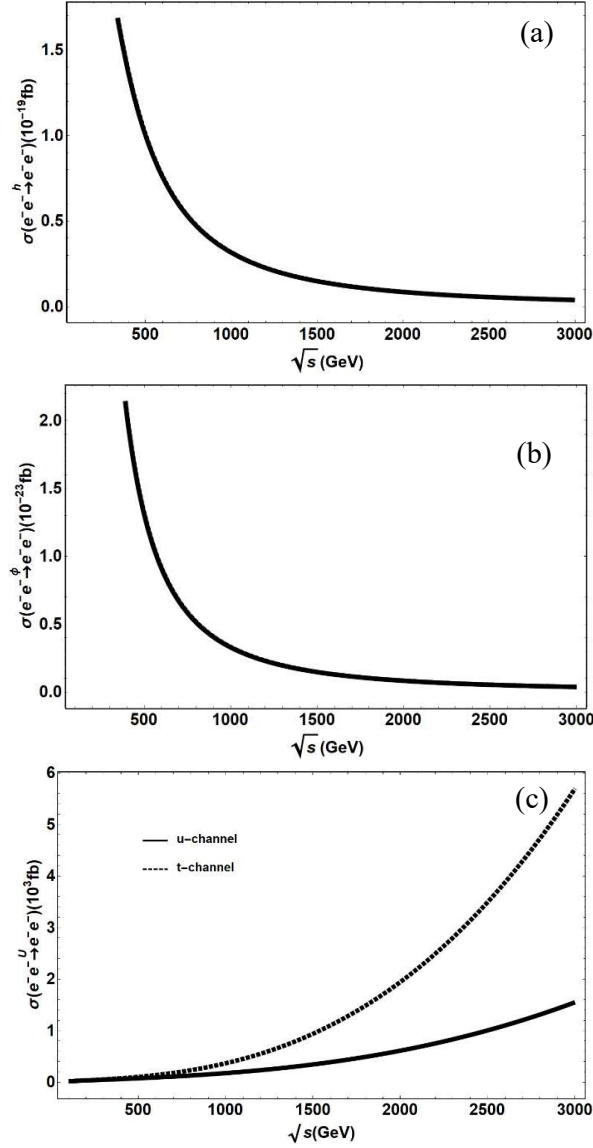
Fig. 4. Total cross-sections as functions of the collision energy via (h, φ, U) exchange.

We have plotted the TCS versus the collision energy $\sqrt{s}$ via (h, φ, U) exchange. Higgs-radion exchange contribution is negligible in the process. In Fig. 4a and 4b, one can find that the TCSs of (h, φ) exchange have the same values in accordance with the energy $\sqrt{s}$. In contrast to the scalar unparticle exchange, the contribution from Higgs-radion rules the low energy region. The important point noted here is that the scalar unparticle effect in RS model on the final state is more observable in higher energy region above 1.5 TeV.

   In the rest of the calculations, we continue studying the process under cases of the polarized e^-e^- beams. For γ exchange, we obtained polarized cases for the initial state with left-handed (*LL*) or right-handed (*RR*) incoming e^-e^- beams and the final state with left-handed (*LL*) or right-handed (*RR*) outgoing e^-e^- beams, respectively.

   Significant results for *Z* boson exchange, with only the initial state of *LL, RR* of incoming e^-e^- and the corresponding final state of *LL, RR* of outgoing e^-e^-, are shown. Regarding vector unparticles, the DCS value is meaningful when the polarized states of the particle beams are right-handed (*RR*) (Fig. 5d).
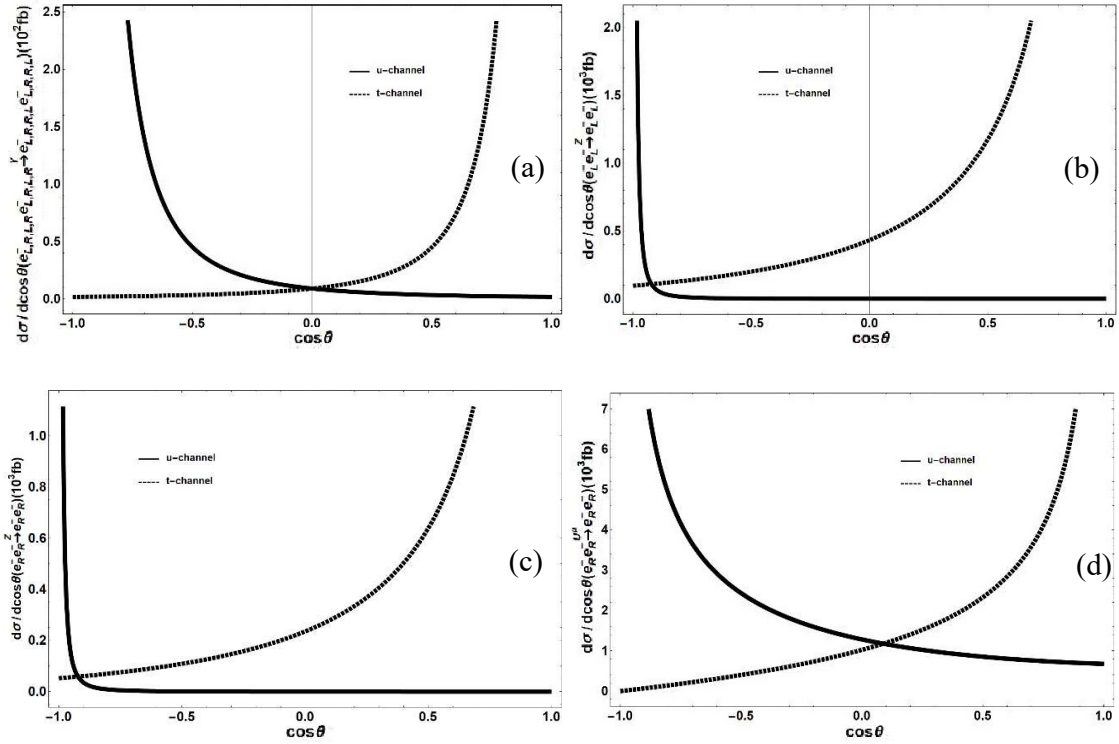
Fig. 5. Differential cross-sections as functions of $\cos\theta$ in u- and t-channel via (γ, Z, U^μ) exchange in polarized cases of the particle beams both initial and final state.

   The figures of values of DCS in every possible polarized cases show us that the directions of observation would be opposite in both channel u and t via every exchange photon γ, boson *Z* and vector unparticles U^μ (Fig. 5). *Z* boson and vector unparticle exchange dominate the process, with the highest values of DCS being observed via *Z* exchange when $\cos\theta$ lies in the intervals $[-0.9, -0.8]$ and $[0.8, 0.9]$ (Figs. 5b and 5c).

   Figure 6 indicates that the contribution to DCS is from Higgs-radion exchange in the polarized states of the incoming and outgoing e^-e^- beams which are mixed between left-handed and right-handed particle (*LR, RL*). Towards scalar unparticle exchange, we only consider the mixed polarized states *LR* and *RL* for the incoming and outgoing e^-e^- beams respectively owing to small contribution from the other mixed polarized states.

Similarly to the unpolarized case of Higgs-radion, the polarized conditions are of insignificant value (Figs. 6a, 6b). The two channels can also be separated with two observable regions in terms of the DCS. Scalar unparticle U contributes the most to the process via (h, φ, U) exchange. About scalar unparticles, the peak values of DCS reach 80 fb in both channels, with a gradual decline to 0 at the other end of its corresponding function $\cos\theta$ (Fig. 6c).

(a)

(b)

(c)
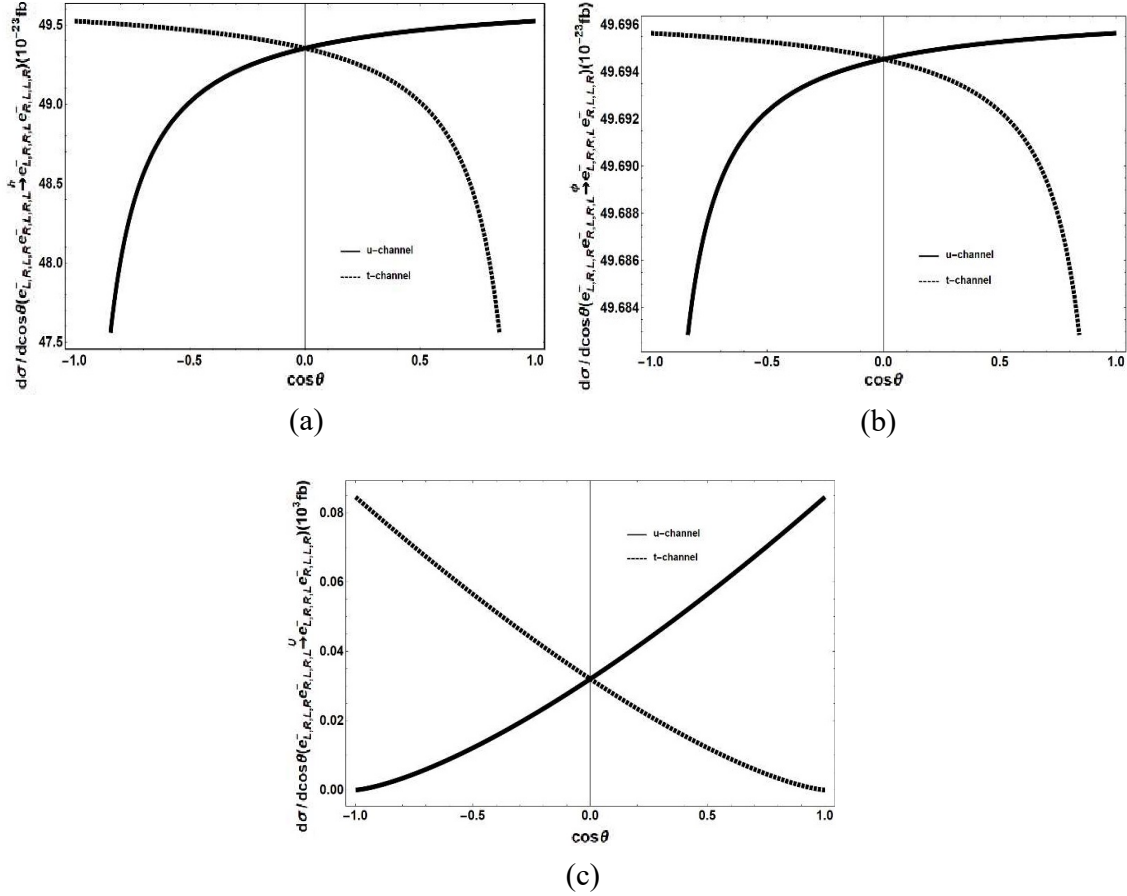
Fig. 6. Differential cross-sections as functions of $\cos\theta$ through u-, t- channel via (h, φ, U) exchange in polarized cases of the particle beams both initial and final state.

In Fig. 7, we investigate the dependence of the total cross-sections (TCS) on the collision energy $\sqrt{s}$ with the polarized conditions of the incoming e^-e^- beams. Figures 7b -7d show that the greatest contributions in very high energy region above 2 TeV arise mostly from Z boson and vector unparticles.

Significantly, the TCSs for LL and RR polarized incoming and outgoing e^-e^- beams γ exchange in both channel are the same in values. Further, the TCS for the left-handed e^-e^- beams in both initial and final states via Z boson exchange in u-channel increases to over $4 \times 10^3 fb$ as $\sqrt{s}$

is reaching the maximum of 3 TeV. The TCS for the process with polarized state $RR\ e^-e^-$ beams via vector unparticle is also more considerable in comparison with other exchanges (Fig. 7b).
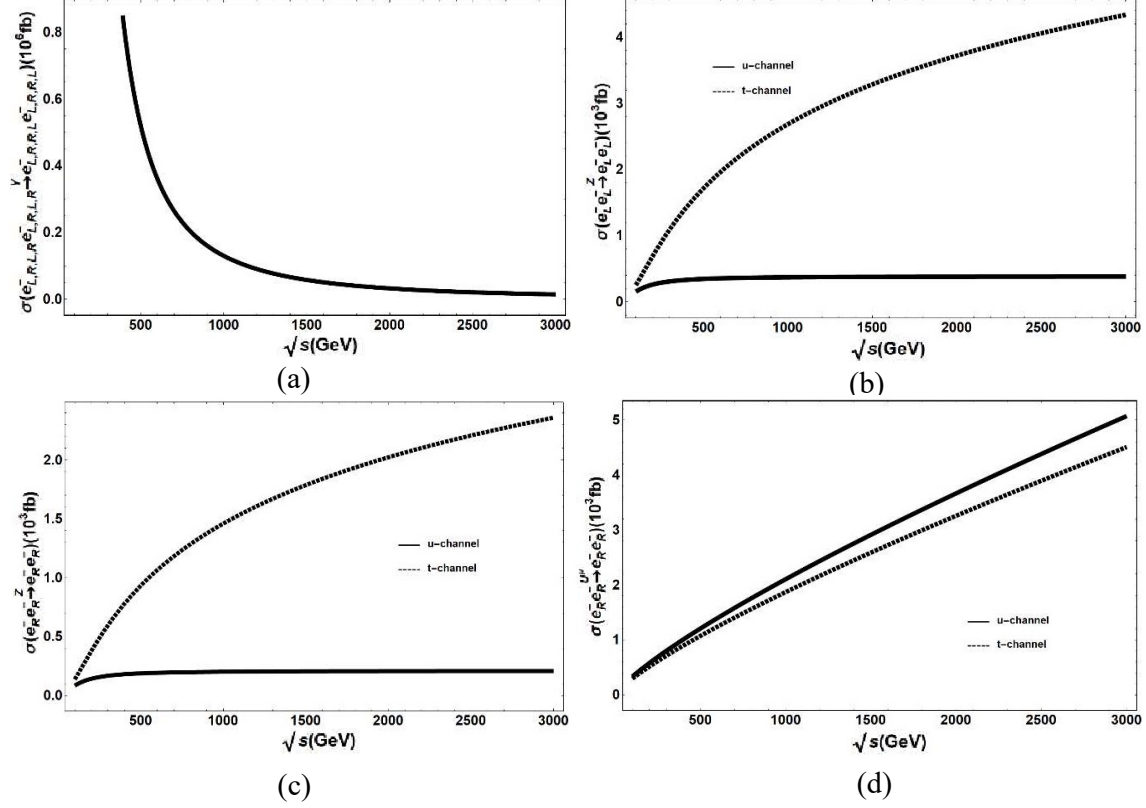
Fig. 7. Total cross-sections as functions of the collision energy via (γ, Z, U^μ) exchange in polarized cases of the particle beams both initial and final state.

Via (h, φ, U) exchange, as can be seen from Figs. 8a-8b, Higgs-radion exchange contributes the most to the process in a low energy region below 0.5 TeV (around $10^{-20}\ fb$). The plots show that the values of TCS in two channels u and t are the same. Scalar unparticle U through both channels has a decent influence in the process throughout the energy regions we investigated (Fig. 8c), likewise, its contribution is less influenced in comparison with vector unparticles. Overall, for the polarized conditions via (γ, Z, U^μ) exchange, when $\cos\theta$ lies in the interval around from -0.8 to 0.8, we have the greatest value of DCS in both u- and t-channel. The pattern is also repeated for (h, φ, U) exchange.

The e^-e^- running mode has been the approachable options of physics at the International Linear Collider (ILC) and Compact Linear Collider (CLIC). Table 1 shows the total cross section (TCS) in terms of the center-of-mass energy in the upcoming potential stages of ILC and CLIC [14–16].

The TCSs decline meanwhile the energy $\sqrt{s}$ increases from 100 GeV to 3 TeV, which apparently implies that the perturbative unitarity of cross-section is not violated. Meanwhile, the
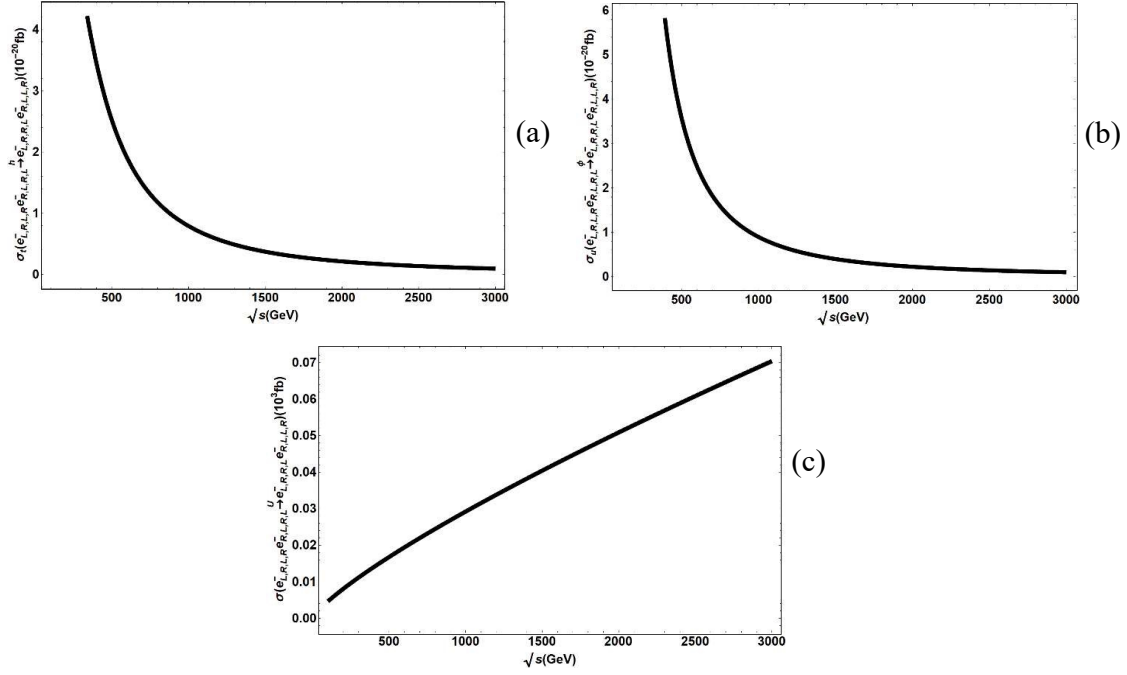
Fig. 8. Total cross-sections as functions of the collision energy via (h, φ, U) exchange in polarized cases of the particle beams both initial and final state.

cross-section contribution from unparticles in very high energy is evidently increasing. The same consequence can also be seen in the Bhabha process studied by H. H. Bang *etal.* [17].

Table 1. Total cross-sections in terms of the specific center-of-mass energy $\sqrt{s}$ at ILC and CLIC. SM, RS and RS(U) stand for Standard Model, Randall-Sundrum Model and Randall-Sundrum with Unparticles, respectively.

$\sqrt{s}$ (GeV)		100	200	500	1000
TCS (mb)	SM	0.103864	0.0259687	0.00416073	0.00104773
	RS	0.103864	0.0259687	0.00416073	0.00104773
	RS(U)	0.103865	0.0259693	0.00416211	0.00105038
$\sqrt{s}$ (GeV)		1500	2000	2500	3000
TCS (mb)	SM	0.000472386	0.000271541	0.000178852	0.000128653
	RS	0.000472386	0.000271541	0.000178852	0.000128653
	RS(U)	0.000476579	0.000277759	0.000187727	0.000140962

Figures 9 and 10 imply that the aforementioned TCSs in SM, RS model and RS model with unparticles decrease along with the energy.
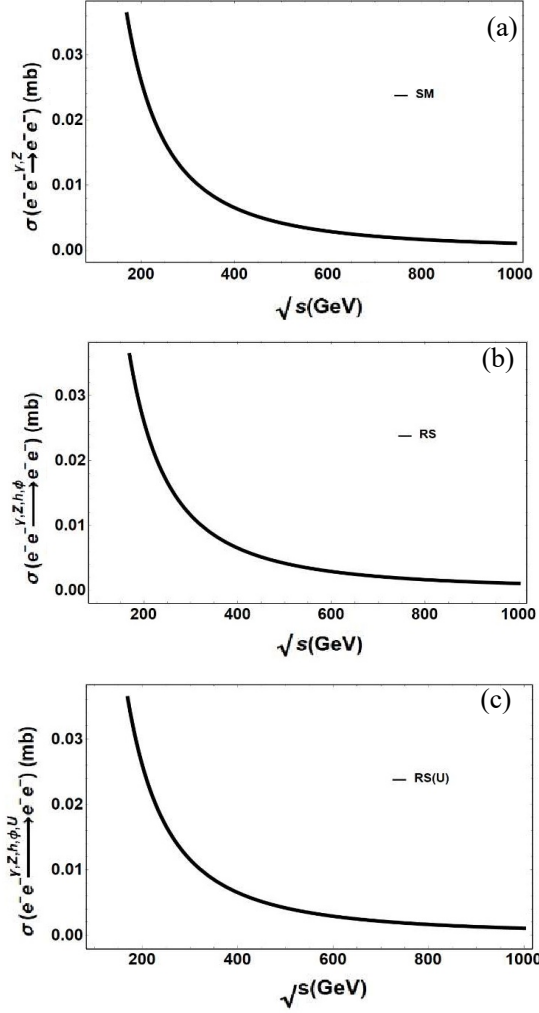
Fig. 9. Total cross sections as functions of the collision energy from 0.1 to 1 TeV in SM, RS model and RS model with unparticles.
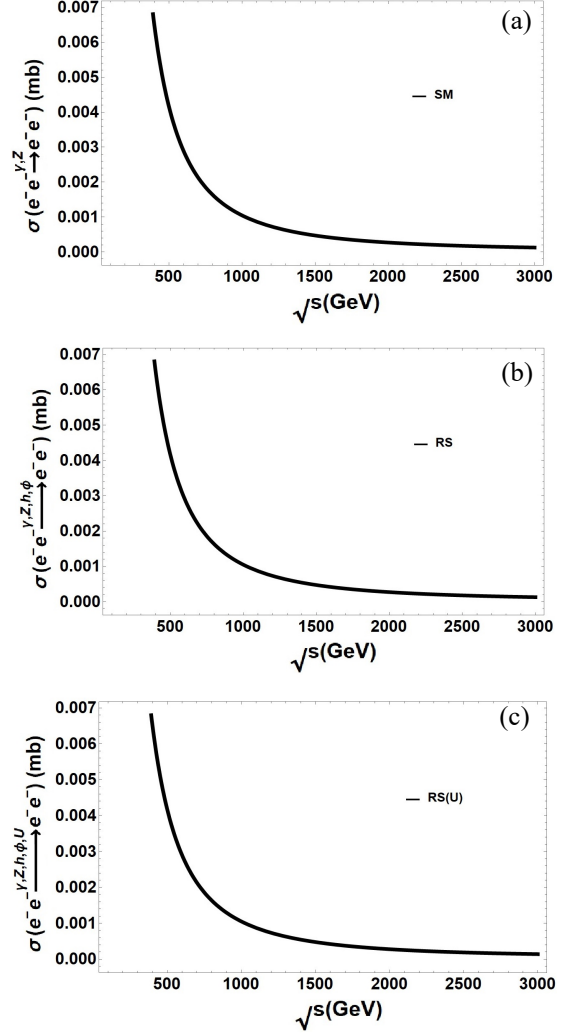
Fig. 10. Total cross-sections as functions of the collision energy from 0.1 to 3 TeV in SM, RS model and RS model with unparticles.

4. Conclusion

The DCS behavior of every exchanges in the SM and RS model profoundly shows the opposite directions in observing the final state of the process through u- and t-channel. Furthermore, the Z boson exchange and unparticles contribute the most to the observable DCS values. On the subject of the TCS, photon and Higgs-radion exchange consistently govern the low energy of the process, while Z boson in t-channel and unparticles, especially vector unparticles U^μ, making up most of the TCS observable values in both unpolarized and polarized states of the e^-e^- beams. Z boson exchange and unparticles govern the process in the high energy region from 1 to 3 TeV,

with Z boson contribution in the left-handed polarized beams being the largest through t-channel as the e^-e^- unpolarized. Moreover, the unparticle effect becomes universal throughout the higher collision energy $\sqrt{s}$ that is larger than 1 TeV.

References

[1] P. L. Anthony *et al.*, [SLAC E158 Collaboration], *Precision measurement of the weak mixing angle in Moller scattering*, Phys. Rev. Lett. **95** (2005) 081601; [arXiv:hep-ex/0504049v1]

[2] J. Benesch, P. Brindza, R. D. Carlini, J-P. Chen, E. Chudakov, S. Covrig *et al.*, [The MOLLER Collaboration], *The MOLLER Experiment: An ultra-precise measurement of the weak mixing angle using Møller scattering*, 2014; [arXiv:1411.4088v2]

[3] J. Balewski, J. Bernauer, W. Bertozzi, J. Bessuille, B. Buck, R. Cowan *et al.*, *A Proposal for the darkLight experiment at the Jefferson Laboratory free Electron Laser* PAC39, 2012.

[4] A. Schmidt, C. O'Connor, J.C. Bernauer and R. Milner, *A novel technique for determining luminosity in electron-scattering/positron-scattering experiments from multi-interaction events* Nucl. Instr. Meth. A **877** (2018) 112.

[5] M. Meziane *et al.*, (The PRad Collaboration), *High precision measurement of the proton charge radius: The PRad experiment*, AIP Conf. Proc. **1563** (2013) 183.

[6] L. Randall, R. Sundrum, *Large mass hierarchy from a small extra dimension*, Phys. Rev. Lett. **83** (1999) 3370.

[7] D. Dominici, B. Grzadkowski, J. F. Gunion and M. Toharia, *The scalar sector of the Randall–Sundrum model*, Nucl. Phys. B **671** (2003) 243; [arXiv:hep-ph/0206192]

[8] Daniele Dominici, Bohdan Grzadkrowski, John F. Gunion and Manuel Toharia, *Higgs-Boson interactions within the Randall-Sundrum model*, Acta Phys. Polon. B **33** (2002) 2507; [arXiv:hep-ph/0206197v1].

[9] M.E. Peskin, D.V. Schroeder, *An introduction to quantum field theory*, Addision-Wesley Publishing, 2018.

[10] D. V. Soa, D. T. L. Thuy, N. H. Thao and T. D. Tham, *Radion production in γe^- collisions*, Mod. Phys. Lett. A **27** (2012) 1250126.

[11] A. Friedland, M. Giannotti and M. Graesser, *On the RS2 realization of unparticles*, Phys. Lett. **B 678** (2009) 149.

[12] D. V. Soa and B. T. H. Giang, *The effect of the scalar unparticle on the production of Higgs–radion at high energy colliders*, Nucl. Phys. **B 936** (2018) 1.

[13] D. V. Soa and B. T. H. Giang, *The influence of the scalar unparticle on the W-pair production at ILC in the Randall Sundrum model*, Mod. Phys. Lett. **A35** (2020) 25.

[14] Brau, James and Okada, Yasuhiro and Walker, Nicholas J and Djouadi, Abdelhak and Lykken, Joseph and Monig, Klaus and Oreglia, Mark and Yamashita, Satoru and Phinney, Nan and Toge, Nobukazu and Behnke, Ties and Damerell, Chris and Jaros, John and Miyamoto, Akiya, *International Linear Collider reference design report: ILC Global Design Effort and World Wide Study*, CERN Yellow Reports: Monographs, 2007, 10.5170/CERN-2007-006.

[15] Abdelhak Djouadi, Joseph Lykken, Klaus Mönig, Yasuhiro Okada, Mark Oreglia and Satoru Yamashita, *et al.*, *International Linear Collider Reference Design Report Volume 2: PHYSICS AT THE ILC*, arXiv:0709.1893 [hep-ph]

[16] M. Aicheler, P.N. Burrows, N. Catalan, R. Corsini, M. Draper, J. Osborne *et al.*, *The compact linear collider (CLIC) - Project implementation plan*, 2019, [arXiv:1903.08655v1]

[17] Sa Thi Lan Anh, Trieu Quynh Trang, Nguyen Thu Huong, and Ha Huy Bang, *Unparticle effects on Bhabha scattering*, Canadian Journal of Physics **96** (2018) 268.